To cite this article: NI B Y, XU Y, HUANG Q, et al. Application of improved cohesive zone length formula in ice mode I crack propagation[J/OL]. Chinese Journal of Ship Research, 2022, 17(3). http://www.ship-research.com/en/article/doi/10.19693/j.issn.1673-3185.02701.

DOI: 10.19693/j.issn.1673-3185.02701

Application of improved cohesive zone length formula in ice mode I crack propagation

NI Baoyu[*1], *XU Ying*[2], *HUANG Qi*[3], *YOU Jia*[1], *XUE Yanzhuo*[1]

1 College of Shipbuilding Engineering, Harbin Engineering University, Harbin 150001, China

2 Marine Design and Research Institute of China, Shanghai 200011, China

3 Jiangsu Branch of China Classification Society, Nanjing 210011, China

Abstract: [**Objectives**] The cohesive zone length is the sum of the cohesive element length at the failure edge and the lengths of the other cohesive elements connected to it. The cohesive zone length determines the maximum size of the mesh. Therefore, the accurate estimation of cohesive zone length and reasonable mesh division are important factors affecting calculation accuracy. [**Methods**] Based on several *J*-integral assumptions and existing research results, a modified function on length thickness ratio value is added to the original formula. The modified formula is then applied to an ice mechanics model. Based on the finite element method, a model of a double cantilever beam is established to verify the accuracy of the formula through comparison with the experimental results. [**Results**] The results show that there must be at least four cohesive elements in a cohesive zone length to describe the fracture process accurately. This conclusion is also applied to the numerical simulation of a three-point bending experiment. The error of the limit load is 2.9%, and that of the fracture point is within a reasonable range. [**Conclusion**] It is concluded that the modified cohesive zone length formula is more suitable for ice materials.

Key words: ice mechanics; cohesive element method (CEM); cohesive zone length; mesh division; three-point bending experiment

CLC number: U661.1

0 Introduction

The study of the collision between structures and ice has received widespread attention in the fields of the design and manufacture of structures for ice regions, the development and utilization of resources in polar regions, and the safe navigation and operation of ships and structures in ice regions. Currently, the methods extensively used for the study of structure-ice collisions include the discrete element method [1-2] and the finite element method [3]. Thereinto, the discrete element method has certain advantages in the study of ice crack propagation, but it is not sufficient for the study of sea ice deformation; the finite element method is relatively mature for the simulation of sea ice and structural deformation, but it is not accurate for the simulation of ice crack propagation. For this reason, some re-

Received: 2021 − 12 − 14 **Accepted:** 2021 − 04 − 07

Supported by: National Natural Science Foundation of China (52192693, 52192690, 51979051, 51979056)

Authors: NI Baoyu, male, born in 1986, Ph.D., professor. Research interest: ice-water-ship coupling kinematics.
E-mail: nibaoyu@hrbeu.edu.cn
XU Ying, female, born in 1991, Ph.D., engineer
HUANG Qi, male, born in 1994, master degree, assistant engineer. Research interest: ice load.
E-mail: qhuang@ccs.org.cn
YOU Jia, male, born in 1997, master degree candidate. Research interest: ice-structure interaction.
E-mail: you20150122@hrbeu.edu.cn
XUE Yanzhuo, male, born in 1978, Ph.D., professor. Research interest: polar ship design and manufacture.
E-mail: xueyanzhuo@hrbeu.edu.cn

***Corresponding author:** NI Baoyu

searchers applied the cohesive element method (CEM) to the simulation of ice cracks. The CEM is a dedicated finite element method of simulating crack initiation and propagation in numerical models, and it can be traced back to the development and study of the Dugdale-Barenblatt (D-B) [4-5] model of crack tips by researchers. The original idea for the cohesion model is the atomic traction-separation law proposed by Barenblatt [5], and the law could be applied to avoid unrealistic stress singularities at the crack tip. Later, Dugdale [4] used the cohesion model to describe the plastic deformation of an ideal elastoplastic material subjected to normal stress in the vicinity of the crack tip. Then, Needleman [6] referred to the crack region in the D-B model as the cohesive zone. The cohesion model has been improved by many researchers and has been applied in many fields. Compared with other crack calculation models, the cohesion model has the advantage of being able to simulate multiple crack paths and thus save the effort of crack path tracking. In addition, the propagation of the crack path can be simulated by arbitrarily placing cohesive elements without knowing the direction of crack propagation in advance. This paper focuses on the application of the CEM in ice crack propagation as it is of great significance for the design and manufacture of structures in ice regions.

Due to its advantages in crack propagation and material fracture, the cohesion model has increasingly been applied to the simulation of ice mechanics and structure-ice collisions in recent years. For example, Mulmule [7] and Dempsey [8] used the ice material with the mode Ⅰ fracture pattern to inversely calculate the cohesion law; Kuutti et al. [9] simulated the experimental collision between vertical steel plates and thick ice blocks by inserting two-dimensional cohesive elements around the triangular ice elements and found that the finite element model with dense meshes could better simulate the failure process of the ice blocks in the experiment; both Lu et al. [10] and Wang et al. [11] employed the CEM to simulate the collision between cones and level ice; Wang et al. [12], Liu et al. [13], and Jiang et al. [14] applied the CEM to simulate the collision of flat ice with vertical cylinders, offshore platforms, and other offshore structures and verified the reliability of the CEM in dealing with such collision problems.

Currently, although the CEM has been applied to the study of structure-ice interaction, the cohesive zone length formula for ice is rarely investigated. Some researchers directly adopted the formulas for other materials. For example, Lu et al. [10] preliminarily estimated the cohesive zone length with the formula for elastic material and an ice crack experiment. However, most researchers have not paid attention to the calculation of the cohesive zone length. For example, Gürtner et al. [15], Kuutti et al. [9], and Wang et al. [11] all failed to mention the relationship between cohesive zone length and meshes and mostly adopted the trial-and-error method for mesh division when they were dealing with various structure-ice collision problems. In fact, the results of research on other materials are not necessarily applicable to ice, and previous studies of cohesive zone length have mainly focused on small-thickness models [16-17], such as the interlayer of composite materials, with little attention paid to large-thickness models. In terms of ice fracture pattern, ice is usually a large-thickness model, so the existing cohesive zone length applicable to thin plates no longer applies to ice.

Regarding the deficiencies in the above studies, this paper presents a new applicability study of cohesive zone length calculation and mesh division of ice materials. Specifically, the existing cohesive zone length formula was reproduced, derived, and modified; then, simulation was conducted with a numerical model of a double cantilever beam built by the finite element method to study the mesh density of the finite element model within the length of a single cohesive zone; finally, the relevant results were applied to a three-point bending experiment of ice with the LS-DYNA software to verify the validity of the CEM in simulating the mode Ⅰ crack initiation and propagation in ice. This paper is expected to promote the application of the CEM in the study of the mechanical properties of ice materials.

1 Cohesive zone length formula and its principle

The CEM has been mainly applied to concrete structures and composite materials after it was proposed. It demonstrates excellent crack simulation capability. Specifically, it can visually simulate the process of cracking and failure, such as opening, sliding, and tearing, of materials, and well simulate the cracking process of concrete and the delamination failure process of composite materials. At present, the common traction-separation relationship controlling the cohesive zone has four forms: bilinear [18], polynomial [19], trapezoidal[20], and exponen-

tial [21] (Fig. 1). In the figure, σ_0 is the maximum stress of crack formation, δ_n is the upper and lower surface displacement corresponding to damage initiation, δ_f is the upper and lower surface displacement corresponding to the initiation of the linear decline in the "trapezoidal" stress, and δ_0 is the maximum upper and lower surface displacement at the time of crack formation.

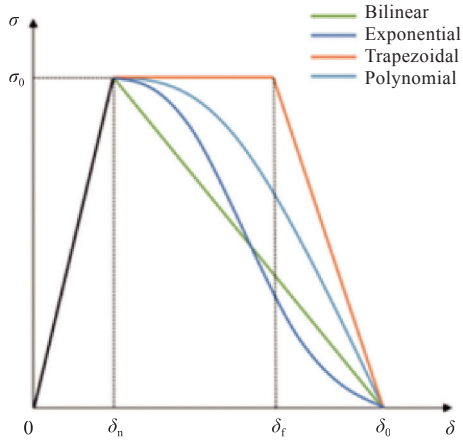

Fig. 1 Traction-separation curves

Fig. 2 presents the directions of cohesion models of different materials. In the figure, the crack propagation direction is defined as the length direction, while the crack opening direction is defined as the thickness direction. The comparison of the two figures indicates that sea ice is a typical large-thickness model.

The cohesive zone length can be derived with the

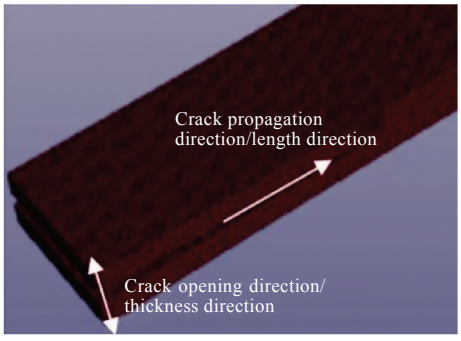

(a) Cohesion model of composite materials (low thickness)

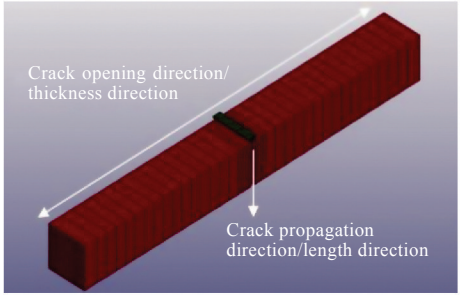

(b) Cohesion model of sea ice (high thickness)

Fig. 2 Direction definition for cohesion models of different materials

J-integral. The *J*-integral, a path-independent integral in elastoplastic fracture mechanics [22], can be used as an average measure of the strain field at the top of a crack or notch. In this paper, the model of a double cantilever beam with opening failure was applied to briefly describe the process of deriving the length of the crack propagation zone (Fig. 3). In the figure, L_{cz} is the length of the crack propagation zone (namely, the cohesive zone length), L is the length of the double cantilever beam without the initial crack, L_{pc} is the length of the initial crack, L_0 is the length of the entire double cantilever beam, and h is the thickness of a single cantilever beam. The initial crack at the left end of the double cantilever beam was used to constrain the generation position and propagation direction of the crack, and the external torque M was applied to the left end of the double cantilever beam.

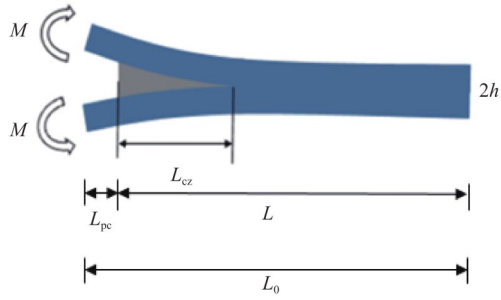

Fig. 3 Tearing of double cantilever beam

The loop integral of the *J*-integral is defined by the following equation [22]:

$$J = \int_{\Gamma} w\mathrm{d}y' - \bar{\boldsymbol{T}}\frac{\partial \bar{\boldsymbol{u}}}{\partial x'}\cdot \mathrm{d}s \tag{1}$$

where w is the strain energy density; Γ is the curve that begins to rotate counterclockwise from a point on the lower surface of the crack to any point on its upper surface; (x', y') is the coordinate of a point on the curve; $\bar{\boldsymbol{T}}$ is the stress vector on the integral loop; $\bar{\boldsymbol{u}}$ is the displacement vector at each point in the loop; ds is the line element along the loop.

The double cantilever beam model shown in Fig. 3, Eq. (1), and the conservation of *J*-integral together support the following equation:

$$\frac{12M^2}{Eh^3} - \sigma_0\delta_0 = 0 \tag{2}$$

where $M = 0.5aL_{cz}^2\sigma_0$ is the relationship between the external torque M and the stress in the crack, with the dimensionless coefficient a related to L and h. The above equation is derived without considering the initial energy under the condition that the length-to-thickness ratio L/h is larger than one. In the equation, the first term is the work done by the external

torque M, and the latter term is the energy within the structure. The two are equal without considering the body force and unloading. The relationship between the external torque M and the stress in the crack is substituted into Eq. (2) for further simplification, thus obtaining

$$L_{cz} = a^{-\frac{1}{2}}\left(\frac{E\delta_0}{3\sigma_0}\right)^{\frac{1}{4}} h^{\frac{3}{4}} \tag{3}$$

All the constant coefficients (terms containing the dimensionless coefficient a and constant terms) can be unified and replaced with characters to generalize the formula. For this purpose, Eq. (3) can be further transformed into

$$L_{cz} = c\left(\frac{E\delta_0}{\sigma_0}\right)^{\frac{1}{4}} h^{\frac{3}{4}} \tag{4}$$

where c is the dimensionless coefficient related to L and h.

Eq. (4) can be further simplified as

$$L_{cz} = c(c_2)^{\frac{1}{4}} h^{\frac{3}{4}} \tag{5}$$

where

$$c_2 = \frac{E\delta_0}{\sigma_0} \tag{6}$$

Hillerborg et al. [23] derived the relationship of the length of the original crack propagation zone with the crack displacement and stress with the D-B model as

$$\tilde{L}_{cz} = \frac{E\delta_0}{f} = \frac{1}{k}\frac{EG}{f^2} \tag{7}$$

where f is the maximum stress at the time of crack formation and is equivalent to σ_0 in Eq. (6), that is, $f = \sigma_0$; $G = k\delta_0 f$ is the fracture energy release rate with a constant k. Applicable to mode Ⅰ and mode Ⅱ fracture patterns, G can be interpreted as the area enclosed by each curve and the coordinate system in Fig. 1, and it can also be expressed as the product of the maximum stress, the maximum strain, and a constant. A comparison between Eq. (6) and Eq. (7) reveals that the $\tilde{L}_{cz}$ in Ref. [23] is consistent with c_2 in Eq. (6) and is equally applicable to tearing (mode Ⅰ tensile failure of cohesive elements) failure. Therefore, Eq. (5) can be modified as

$$L_{cz} = c_1\left(\frac{EG}{\sigma_0^2}\right)^{\frac{1}{4}} h^{\frac{3}{4}} \tag{8}$$

The above derivation is originally for the crack propagation and the calculation of the crack zone length of composite materials. However, since the type and properties of the material are not restricted, the above-mentioned idea of crack description also applies to the mode Ⅰ crack initiation and propagation in ice. The bilinear δ-σ curve mentioned in Ref. [23] is suitable for such brittle or quasi-brittle materials as concrete. This paper also used the bilinear δ-σ curve for ice mechanics simulation by the CEM.

The selection of the coefficient c_1 is a major difficulty in the application of Eq. (8). Previous related researchers mainly focused on thin plate models and recommended different values, such as 0.5 [24], $\pi/8$, 0.731, and 2.92 [25], for c_1 according to material properties and the constitutive relation of the cohesion model. However, all these parameters are simple fixed values, ignoring the feature of c_1 that it varies with model size. Moreover, they are only readily applicable to thin plate materials with small thicknesses (Fig. 2 (a)). In contrast, their applicability to ice materials with large thicknesses (Fig. 2 (b)) has not been reported by relevant literature. Therefore, the value of the coefficient c_1 applied to ice materials is discussed in this paper.

2 Cohesive zone length applied to ice materials

In this paper, the change law of the cohesive zone length L_{cz} with model size was discussed before a modified formula of the coefficient c_1 was presented. Two values were concerned here, namely, the thickness h and the length-to-thickness ratio L/h. In the finite element model, the failure of the elements can be judged by whether the stress on the elements or strain of the elements exceeds the set value in the model [26]. In this paper, the deformation displacement of the cohesive elements was calculated by tracking the coordinates of the element nodes at each moment. In light of the displacement law, the change in the node's coordinates was used to determine whether the cohesive element was in an irreversible deformation state, and the failure of the cohesive element was further determined according to the traction-separation curve (Fig. 1). The time interval of coordinate data output was reduced as much as possible and finally set to 5×10^{-5} s to reduce the error.

A numerical model of a double cantilever beam was built, with the entire length L_0=150 mm of the double cantilever and the thickness h =1.55 mm of a single cantilever beam. The force-bearing end of the model has a notch with an initial crack length L_{pc}=35 mm, and the length of the double cantilever beam without initial cracks is L=115 mm. The crack propagation length was set to the cohesive zone length L_{cz}, and the double cantilever beam was sub-

jected to tensile forces F of equal magnitude in opposite directions. The tensile deformation of the cohesive element in the model is shown in Fig. 4. The figure reveals that when the loading time increases from 0 s to 0.35 s, tensile deformation of the cohesive element gradually takes place as the force loading continues, and when the loading time reaches 0.5 s, the cohesive element reaches its force-bearing limit and fails.

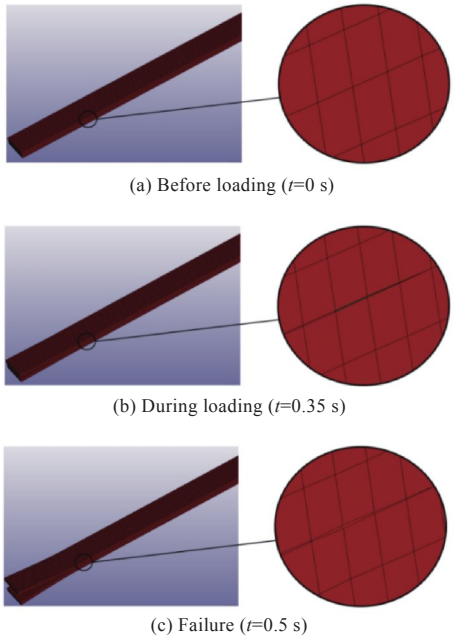

(a) Before loading (t=0 s)

(b) During loading (t=0.35 s)

(c) Failure (t=0.5 s)

Fig. 4 Tensile deformation of cohesive elements

The variation curve of the cohesive zone length L_{cz} with the thickness h of a single cantilever beam during the failure of the double cantilever beam was plotted (Fig. 5) under an invariant initial crack length L_{pc}=35 mm and a variable length L(115, 100, and 85 mm) of the double cantilever beam without initial cracks. The variation curve of L_{cz} with $Ln(L/h)$ was further plotted (Fig. 6).

In Fig. 5, the overall cohesive zone length L_{cz} increases gradually with the increase in the length L of the double cantilever beam without initial cracks. As the thickness h of the single cantilever beam increases, the change rate of L_{cz} relative to the increase in h decreases gradually. When h increases to a certain value, L_{cz} basically stops changing. Nevertheless, h affects the change in L_{cz} under a low thickness significantly.

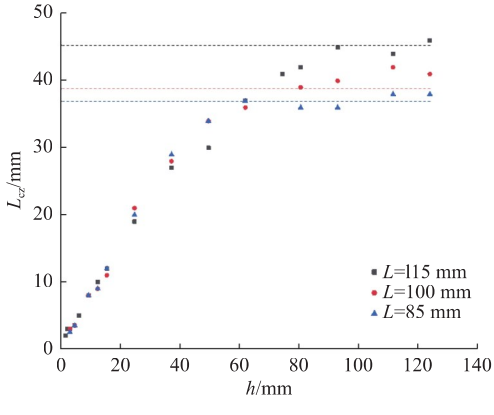

Fig. 5 L_{cz}-h curve

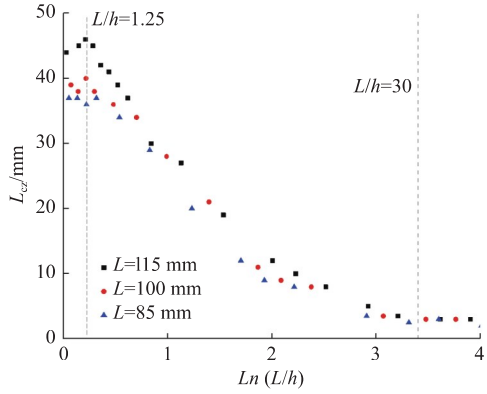

Fig. 6 L_{cz}-$Ln((L/h)$ curve

According to Fig. 6, the influence of the increase in the length-to-thickness ratio L/h on L_{cz} also demonstrates an obvious downward trend. When L/h > 30 ($Ln(30) \approx 3.40$), L_{cz} basically no longer changes; when L/h decreases, L_{cz} gradually becomes sensitive to the change in L/h; when L/h further decreases to L/h<1.25 ($Ln(1.25) \approx 0.223$), L_{cz} fluctuates around a certain stable value again, and the point where this phenomenon occurs is called the inflection point in this paper. Regarding the three models of the double cantilever beam without initial cracks of different lengths L, L/h is all around 1.25 when the inflection point appears. Fig. 5 and Fig. 6 indicate that when L/h is in the range of 1.25 to 30, L_{cz} is clearly affected by the change in L/h; when L/h is not within this range, its effect on L_{cz} is relatively small.

3 Modification of cohesive zone length formula

At present, the CEM is mainly applied to the study of the mechanical properties of thin composite materials with large L/h[16]. The coefficient modification of the cohesive zone length formula mainly involves constant term modification, without considering the phenomenon that the cohesive zone length no longer changes with thickness when the length-to-thickness ratio L/h changes from 1.25 to 1. In the actual simulation, however, the inflection point of the variation of the cohesive zone length, that is, the phenomenon that the change in the cohe-

sive zone length is no longer obvious after L/h reaches a certain value, should be considered. This paper attempts to modify the coefficient c_1 on the basis of previous studies and correlate it with the change in L/h to improve the accuracy of the cohesive zone length formula.

According to the models of the double cantilever beam without initial cracks of different lengths L, the value range of L/h larger than 1.25 was selected, and c_1 was assumed to be a function of L and h. Then, the L_{cz}-h scatter points in the simulation were fitted several times according to Eq. (8) to establish the relationship between c_1 and L/h. The following equation can be obtained by data fitting and sorting:

$$c_1 = \begin{cases} \dfrac{1}{2.2 + \dfrac{0.11x}{L/h_{\min}}}, & (x > 1.25) \\ \dfrac{1}{2.2 + \dfrac{0.137\,5}{L/h_{\min}}}, & (x \leqslant 1.25) \end{cases} \tag{9}$$

Substituting it into Eq. (8), a new cohesive zone length formula can be obtained as

$$L_{cz} = \begin{cases} \dfrac{1}{2.2 + \dfrac{0.11x}{L/h_{\min}}} \cdot \left(\dfrac{EG}{\sigma_0^2}\right)^{\frac{1}{4}} \cdot h^{\frac{3}{4}}, (x > 1.25) \\ \dfrac{1}{2.2 + \dfrac{0.137\,5}{L/h_{\min}}} \cdot \left(\dfrac{EG}{\sigma_0^2}\right)^{\frac{1}{4}} \cdot h^{\frac{3}{4}}, (x \leqslant 1.25) \end{cases} \tag{10}$$

where x is the current value of L/h; $h_{\min}$ is the minimum model thickness simulated. When $h_{\min}$ is much smaller than the length of the model, it has little influence on the calculation result. For ice materials, no relevant calculation has been found so far. In this paper, $h_{\min}$=1.5 mm was selected with reference to the values of composite materials in Ref. [5] and Ref. [16]. For the mode Ⅰ crack initiation and propagation in ice, σ_0 was taken as the tensile strength of the ice, and its value was selected with reference to the tensile test of ice [27]. In addition, as mentioned in the previous section, the cohesive zone length basically stops changing after the inflection point appears. Therefore, this formula is only applicable to the case where L/h is larger than 1.25. For the case where L/h is smaller than 1.25, the cohesive zone length corresponding to L/h =1.25 was taken.

The effectiveness of the modification of the coefficient c_1 on the result of cohesive zone calculation was verified as follows. Numerical models of large-thickness double cantilever beams were reconstructed (Fig. 7). Their width B is 20 mm; their length L are respectively 70 and 210 mm; L_{pc} is still 35 mm; their thickness $2h$ changes continuously. Certain scatter points in the range of L/h from 1 to 150 were selected properly to plot the corresponding curves, and the model calculation results were compared with the results of the modified formula (Fig. 8).

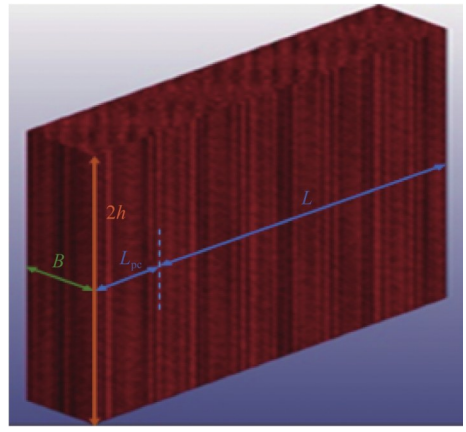

Fig. 7 Double cantilever beam model with large thickness

Fig. 8 shows that regarding the two models of different sizes, the simulation results of the modified model well agree with the direct simulation results over the whole value range of L/h. The analysis not only verifies the validity of the formula but also indicates that the cohesive zone length at the inflection point (L/h = 1.25, namely, the position of the dotted lines in Fig. 8 (a)) is related to the entire length of the double cantilever beam model as well. With the increases in the entire length and the cohesive zone length, the error between the calculation results of the formula and the simulation results gradually decreases, which is particularly evident in the range in which L/h is small.

4 Application of modified formula on ice materials

The mesh density determines the calculation amount. A higher density of cohesive elements in the cohesive zone length L_{cz} leads to smoother crack formation and force curve and higher accuracy. Otherwise, the force curve is more likely to have jagged fluctuations. The process of crack formation and force transmission can be well simulated when an appropriate number is set for the cohesive elements within a single cohesive zone. With the above-mentioned L_{cz} calculation method, this section focuses on the mode Ⅰ tensile failure of the cohesive elements to study the number of cohesive elements that should be arranged in one L_{cz}, namely, $L_{cz} = mS_c$ (where S_c is the size of one cohesive element and m is the number of the elements).

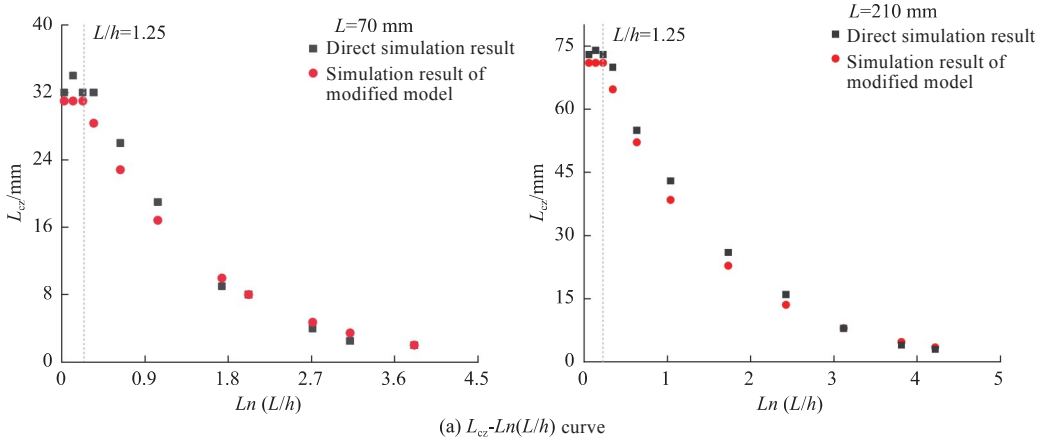

(a) L_{cz}-$Ln(L/h)$ curve

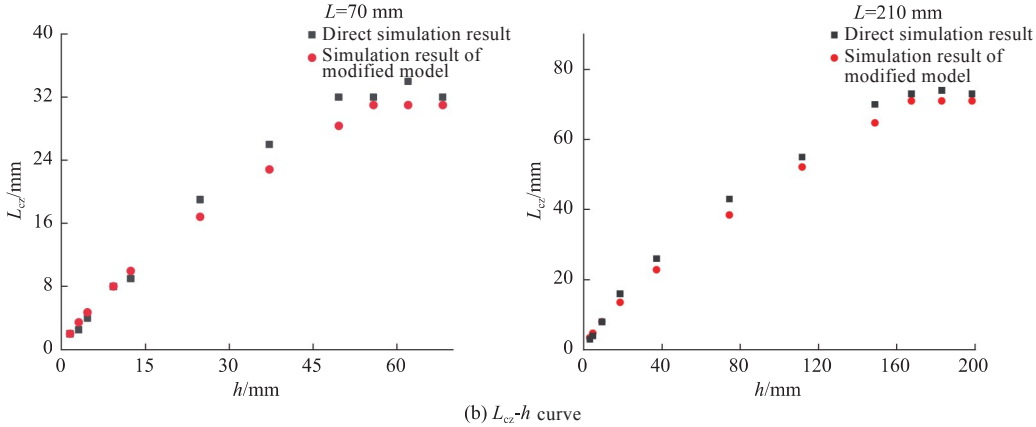

(b) L_{cz}-h curve

Fig. 8 Comparison of simulation results with modified cohesive zone lengths

The main dimensions ($L \times B \times 2h$) of the narrow double cantilever beam model in this section are 150 mm × 20 mm × 3.1 mm (Fig. 9). The ice parameters are as follows: an elastic modulus of 5.72 GPa, a shear modulus of 2.2 GPa, a hardening modulus of 4.26 GPa, a volume modulus of 5.26 GPa, and a velocity of upper and lower traction of 0.004 m/s. The mesh size is successively refined from 2.0 mm to 0.5 mm with an interval of 0.05 mm. The mode Ⅰ tensile failure process of the cohesive elements between the narrow double cantilever beam was simulated under tension drive, and the effects of mesh density on the failure tension and displacement curves were tested under different mesh densities, with the results shown in Fig. 10.

As can be seen from Fig. 10, the curve of the traction to be transmitted by the cohesive elements with time gradually tends to smooth out as the meshes are refined. The overall fluctuation gradually flattens out, and the value gradually approaches the middle. With the cohesive zone length L_{cz}=2 mm calculated from Eq. (10) and the above model data, a cohesive zone length of around 2 mm was obtained by actual simulation.

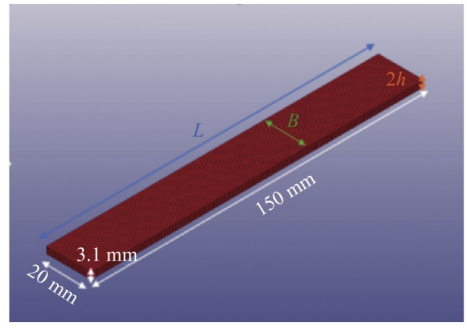

Fig. 9 Main dimensions of narrow double cantilever beam model

According to the distribution of traction-time curves under different mesh densities shown in Fig. 10, the fluctuation of the curve is basically acceptable, and the calculation amount required in the case of a mesh density of 0.5 mm is also acceptable when the mesh size is less than or equal to 0.5 mm. In summary, at least four cohesive elements in one cohesive zone length are required to describe the fracture process of the material accurately under the mode Ⅰ tensile failure of the cohesive elements. In this case, the accuracy and stability of the load curve are also well guaranteed.

After the accuracy of the relationship between the mesh length and the model size of the CEM was

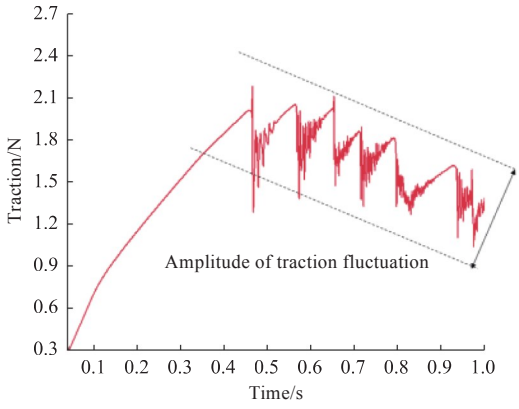

(a) S_c=2.0 mm

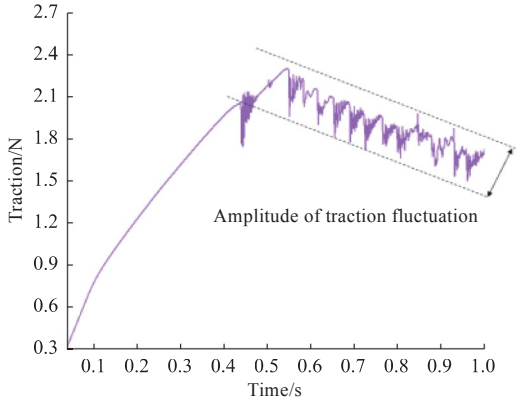

(b) S_c=1.0 mm

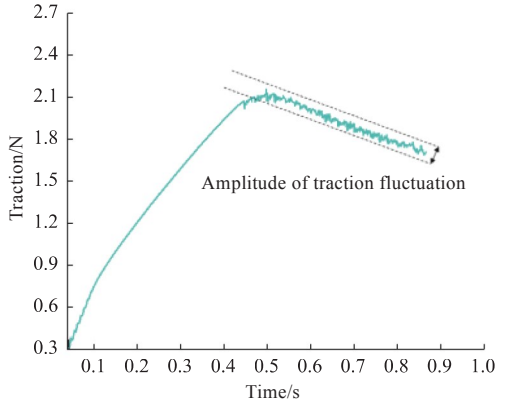

(c) S_c=0.5 mm

Fig. 10 Traction-time curves of cohesive elements with different mesh densities

theoretically deduced and numerically verified, the CEM was employed for a numerical simulation of the three-point bending experiment of ice, thereby presenting the ice change process from deformation to failure. The main dimensions ($L \times B \times 2h$) of the numerical model [28] are 70 mm × 70 mm × 650 mm, and the distance between the fulcrums is 600 mm, as shown in Fig. 11. The relevant parameters are presented in Table 1. The numerical model was built according to the actual experimental model, and the values of ice parameters are derived from the experimental results.

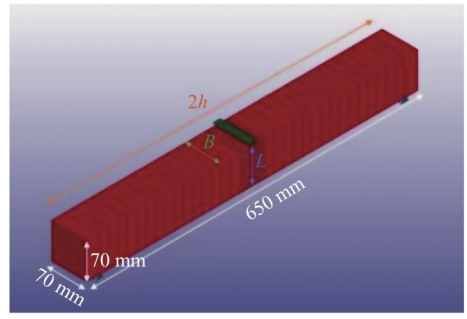

Fig. 11 Main dimensions of ice specimen model

Table 1 Experimental parameters

Parameter	Value
Density / （kg·m^{-3}）	894
Young's modulus / GPa	6.83
Bending strength / MPa	3.2
Poisson's ratio	0.25
Temperature /℃	−10
Strain rate / s^{-1}	4.604×10^{-3}
Ultimate load / N	1 127.9
Ultimate deflection / mm	0.39
Loading duration / s	1.21

For favorable mesh stability and accurate calculation results, the required cohesive zone length L_{cz} was calculated from Eq. (10). In accordance with the crack propagation direction and the definition of the above-mentioned thickness direction in the cohesive zone length formula, the length-to-thickness ratio L/h of the three-point bending experiment model was determined to be about 0.215, which was significantly smaller than the L/h value of 1.25 at the inflection point. Therefore, the L_{cz} value at the inflection point was adopted. L_{cz} = 15.4 mm at the inflection point was obtained by calculation, and the maximum mesh size of the cohesive elements was 3.85 mm according to m = 4.

For the rounding-off mesh division, the length of the cohesive elements in the crack propagation direction was set to 3.5 mm, and that of the cohesive elements perpendicular to the crack propagation direction was set to 4.5 mm during calculation so that a certain amount of calculation can be saved. Under the above mesh density, the calculation step size is 3.68 × 10^{-7} s, and the calculation time is about 4 h.

A finite element model was constructed according to the above experimental data and ice parameters, and cohesive elements were added to the middle part of the specimen that is likely to crack, as shown in Fig. 12. In the figure, the color red represents ice elements, while the color off-white is for

cohesive elements. The ice mechanics model only provided deformation and force transmission, and it was replaced by cohesive elements for ice failure and separation. Therefore, the failure of the ice elements was not taken into account, and only the failure of the cohesive elements was considered. The ice mechanics model was an isotropic linear elasto-plastic model. The numerical simulation process is shown in Fig. 13, and the crack form of the experimental ice specimen is shown in Fig. 14.

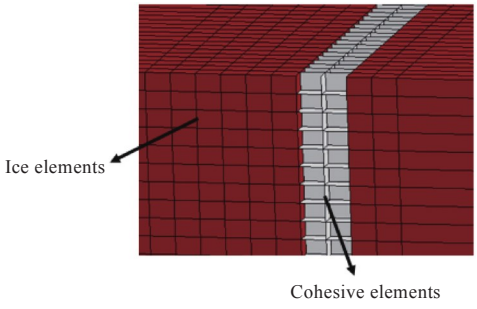

Fig. 12 Cohesive elements between ice specimen sections

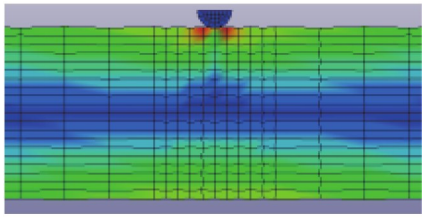

(a) During loading

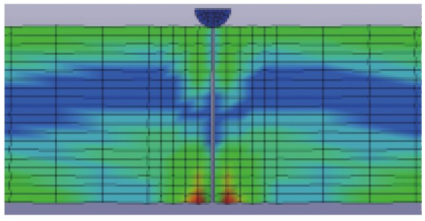

(b) After fracture

Fig. 13 Finite element simulation of three-point bending process

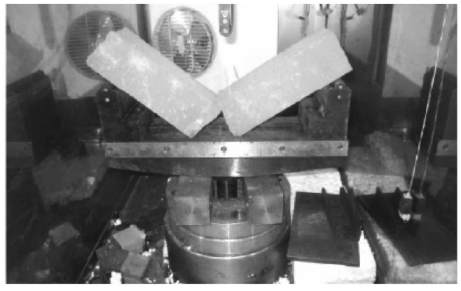

Fig. 14 Fracture of experimental ice specimen [28]

The ice model used in the numerical simulation in this section is uniform. The traction law selected for the cohesive elements was bilinear, and the original defects in the ice specimen were not considered in the construction of the ice mechanics model. Therefore, the ice specimen shown in Fig. 13 has a smooth fracture surface, resulting in smooth ice failure in the overall simulation process. According to the deflection and pressure changes in the object in the numerical simulation, pressure-deflection curves were plotted (Fig. 15).

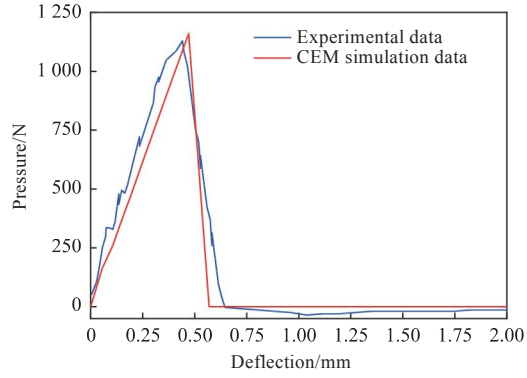

Fig. 15 Pressure-deflection curves

In the experiment, the maximum force on the ice specimen before failure is 1 127.9 N. The ultimate load obtained by the three-point bending simulation based on the CEM is 1 161 N, and the error at the fracture point is thus 2.9%, representing closeness to the experimental result. Regarding the different stages of the pressure-deflection curves shown in Fig. 15, the trend of the curve simulated by the CEM is basically consistent with that of the experimental curve. In terms of the final fracture deflection, the ultimate deflection corresponding to the CEM is of a certain but small error to the experimental data. In addition, since the ice mechanics model selected for the numerical simulation is linear and the original defects are not considered in the process of cohesive element creation, the curve obtained by the simulation is smoother than the one obtained with the experimental data. The comparison between the two curves reveals that the bending deformation and failure processes of the ice specimen in the numerical simulation process are basically consistent with those in the experiment. Moreover, the brittleness of ice and the continuity of crack formation are well reflected by the unloading process after the peak. In summary, the results of the comparison between the simulation data and the experimental data well verify the validity of the CEM and the related mesh division method in simulating the mechanical properties of ice.

5 Conclusion

Proceeding from the *J*-integral, this paper reproduced the derivation process of the cohesive zone

length formula on the basis of several assumptions and relevant previous research results and added a modified function related to the *L/h* value to the original formula cohesive zone length formula. The accuracy of the proposed cohesive zone length formula was verified by the newly built numerical high-thickness model of the double cantilever beam, and the applicability of the formula to the ice mechanics model was thereby solved. A finite element model of the double cantilever beam was constructed for numerical simulation. The results show that at least four cohesive elements in a cohesive zone length are required to describe the fracture process of the material accurately. Finally, the research results were applied to the simulation of the three-point bending experiment model. According to the simulation results, the ultimate load error at the fracture point is 2.9% and within the reasonable range, verifying the validity of the modified cohesive zone length formula in simulating the mode I crack initiation and propagation in ice.

References

[1] LIU L, LONG X, JI S Y. Dilated polyhedra based discrete element method and its application of ice load on cylindrical pile [J]. Chinese Journal of Theoretical and Applied Mechanics,2015,47(6):1046−1057(in Chinese).

[2] DI S C, XUE Y Z, WANG Q, et al. Discrete element simulation of ice loads on narrow conical structures [J]. Ocean Engineering, 2017, 146: 282−297.

[3] WANG J W, ZOU Z J. Ship's structural response during its collision with level ice based on nonlinear finite element method [J]. Journal of Vibration and Shock, 2015, 34 (23): 125−130 (in Chinese).

[4] DUGDALE D S. Yielding of steel sheets containing slits [J]. Journal of the Mechanics and Physics of Solids, 1960, 8 (2): 100−104.

[5] BARENBLATT G I. The mathematical theory of equilibrium cracks in brittle fracture [J]. Advances in Applied Mechanics, 1962, 7: 55−129.

[6] NEEDLEMAN A. A continuum model for void nucleation by inclusion debonding [J]. Journal of Applied Mechanics, 1987, 54 (3): 525−531.

[7] MULMULE S V, DEMPSEY J P. Scale effects on sea ice fracture [J]. Mechanics of Cohesive-Frictional Materials, 1999, 4 (6): 505−524.

[8] MULMULE S V, DEMPSEY J P. A viscoelastic fictitious crack model for the fracture of sea ice [J]. Mechanics of Time-Dependent Materials, 1997, 1(4): 331−356.

[9] KUUTTI J, KOLARI K, MARJAVAARA P. Simulation of ice crushing experiments with cohesive surface methodology [J]. Cold Regions Science and Technology, 2013, 92: 17−28.

[10] LU W J, LØSET S, LUBBAD R. Simulating ice-sloping structure interactions with the cohesive element method [C]//Proceedings of the ASME 31st International Conference on Ocean, Offshore and Arctic Engineering. Rio de Janeiro, Brazil: ASME, 2012.

[11] WANG F, ZOU Z J, GUO H P, et al. Numerical simulations of continuous icebreaking process with different heel angles in level ice[C]//Proceedings of the 37th International Conference on Ocean, Offshore and Arctic Engineering. Madrid, Spain: ASME, 2018.

[12] WANG F, ZOU Z J, REN Y Z. Numerical simulation of level ice-vertical cylinder collision based on a cohesive element model [J]. Journal of Vibration and Shock, 2019, 38 (16): 153−158 (in Chinese).

[13] LIU L P, LI X, XU S W, et al. Numerical simulation of interaction between ice-resistant platform and level ice with cohesive element method [J]. The Ocean Engineering, 2019, 37(2): 20−28 (in Chinese).

[14] JIANG Y Y. Numerical simulation of marine structure-level ice collision based on the cohesive element method [D]. Dalian: Dalian University of Technology, 2020 (in Chinese).

[15] GÜRTNER A, BJERKÅS M, KÜHNLEIN W, et al. Numerical simulation of ice action to a lighthouse[C]// Proceedings of the ASME 28th International Conference on Ocean, Offshore and Arctic Engineering. Honolulu, Hawaii, USA: ASME, 2009.

[16] HARPER P W, HALLETT S R. Cohesive zone length in numerical simulations of composite delamination [J]. Engineering Fracture Mechanics, 2008, 75 (16): 4774−4792.

[17] BAO G, SUO Z. Remarks on crack-bridging concepts [J]. Applied Mechanics Reviews, 1992, 45(8):355−366.

[18] NEEDLEMAN A. Micromechanical modelling of interfacial decohesion [J]. Ultramicroscopy, 1992, 40 (3): 203−214.

[19] TVERGAARD V, HUTCHINSON J W. The influence of plasticity on mixed mode interface toughness [J]. Journal of the Mechanics and Physics of Solids, 1993, 41(6): 1119−1135.

[20] MI Y, CRISFIELD M A, DAVIES G A O, et al. Progressive delamination using interface elements [J]. JournalofCompositeMaterials,1998,32(14):1246−1272.

[21] XU X P, NEEDLEMAN A. Numerical simulations of fast crack growth in brittle solids [J]. Journal of the Mechanics and Physics of Solids,1994,42(9):1397−1434.

[22] LI S Y, HE T M, YIN X C. Rock fracture mechanics [M]. Beijing: Science Press, 2015 (in Chinese).

[23] HILLERBORG A, MODÉER M, PETERSSON P. E. Analysis of crack formation and crack growth in concrete by means of fracture mechanics and finite elements [J]. Cement and Concrete Research, 1976, 6 (6): 773−781.

[24] WANG F, ZOU Z J, ZHOU L, et al. Numerical simulation of ice milling loads on propeller blade with cohesive element method [J]. Brodogradnja, 2019, 70 (1): 109−128.

[25] PLANAS J, ELICES M. Nonlinear fracture of cohesive materials [J]. International Journal of Fracture, 1991, 51 (2): 139−157.

[26] NI B Y, HUANG Q, CHEN W S, et al. Numerical simulation of ice resistance of ship turning in level ice zone considering fluid effects [J]. Chinese Journal of Ship Research, 2020, 15 (2): 1−7 (in Chinese).

[27] TIMCO G W, WEEKS W F. A review of the engineering properties of sea ice [J]. Cold Regions Science and Technology, 2010, 60 (2): 107−129.

[28] XUE Y Z, LU X K, WANG Q, et al. Simulation of three-point bending test of ice based on peridynamic [J]. Journal of Harbin Engineering University, 2018, 39 (4): 607−613 (in Chinese).

修正内聚区长度计算公式在冰I型裂纹扩展中的应用

倪宝玉*[1],徐莹[2],黄其[3],尤嘉[1],薛彦卓[1]

1 哈尔滨工程大学 船舶工程学院,黑龙江 哈尔滨 150001

2 中国船舶及海洋工程设计研究院,上海 200011

3 中国船级社 江苏分社,江苏 南京 210011

摘　要:[**目的**]内聚区长度是处于破坏边缘的内聚力单元长度与其连接的其他内聚力单元长度之和,决定了网格的最大尺寸。精确估算内聚区长度并合理划分网格是影响计算精度的重要因素。[***方法***]为此,基于J积分的部分假设和已有的研究成果,在原有的内聚区长度计算公式中增加关于长厚比的修正函数,然后将修正后的内聚区长度计算公式应用于冰力学模型,再基于有限元法建立双悬臂梁数值模型进行模拟,并与试验结果进行对比,以验证修正后内聚区长度计算公式的精确性。[**结果**]研究表明,在一个内聚区长度内至少存在4个内聚力单元才能较精确地描述断裂过程。相关结果应用于三点弯曲试验模型模拟的结果显示,断裂点的极限载荷误差为2.9%且在合理范围内。[**结论**]修正后的内聚区长度公式更适用于冰材料。

关键词:冰力学;内聚力单元法;内聚区长度;网格划分;三点弯曲试验